Research Square

Preprints are preliminary reports that have not undergone peer review.
They should not be considered conclusive, used to inform clinical practice,
or referenced by the media as validated information.

Layer-by-Layer Antibacterial Coating encompassing Silver Nanoparticles for Infection-Resistant BioHole TM ButtonHole Device

Milan Wouters
University of Antwerp
Laurence Van Moll
University of Antwerp
Florentijn Vandecasteele
University of Antwerp
Zina Bendimouan
University of Antwerp
Linda De Vooght
University of Antwerp
Lukas Van Campenhout
University of Antwerp
Paul Cos
paul.cos@uantwerpen.be

University of Antwerp

Article

Keywords: BioHole™ device, buttonhole cannulation, antimicrobial coating, silver nanoparticles, layer-by-layer assembly, polycarbonate

Posted Date: June 5th, 2026

DOI: https://doi.org/10.21203/rs.3.rs-9557713/v1

License: This work is licensed under a Creative Commons Attribution 4.0 International License.
Read Full License

Additional Declarations: No competing interests reported.

Abstract

Most patients in nephrology units require hemodialysis three times per week. Among the available vascular access techniques, the buttonhole method offers distinct advantages, including improved patient comfort and consistent cannulation. However, its clinical adoption remains constrained by a markedly increased risk of access-related infections. In this study, we present a novel and biocompatible coating strategy for the BioHole™ buttonhole medical device based on in-house produced silver nanoparticles. These particles were uniform, nanosized and monodisperse, exhibiting strong and reproducible antibacterial activity. Following mild aqueous amination of the BioHole™ device surface, a layer-by-layer assembly was applied to deposit a polyelectrolyte multilayer composed of cationic poly-L-lysine and anionic citrate- or citrate/tannic acid-capped silver nanoparticles. The coating demonstrated a strong antibacterial activity against *Staphylococcus aureus* and *Pseudomonas aeruginosa*, while maintaining excellent biocompatibility with L-929 fibroblasts. Overall, this technique provides an effective approach to reduce infection risk during buttonhole cannulation with the BioHole™ device without compromising material performance. On top of that, it offers a versatile strategy for the development of antimicrobial surfaces on polycarbonate-based medical devices.

1. Introduction

Hemodialysis (HD), the most widely used form of renal replacement therapy, serves as a lifeline for patients with kidney failure or acute kidney injury [1]. Effective HD requires reliable vascular access to remove excess fluids and metabolic waste from the bloodstream. Among the available options, arteriovenous fistulas (AVFs) are considered the gold standard due to their long-term reliability and lower infection rates compared to grafts or catheters [2, 3]. Three distinct cannulation techniques are commonly used for AVFs, as illustrated in Fig. 1A: the rope ladder, area, and buttonhole (BH) methods [4, 5]. Rope ladder cannulation involves sharp needle punctures along the entire length of the AVF, while in area cannulation, a small area is repeatedly punctured with sharp needles[6, 7] The BH technique, first introduced by Dr. Twardowski in 1972, relies on the gradual formation of a stable fibrous tract composed of scar tissue, typically developed over approximately 12 weeks [8]. This tract enables repeated cannulation using blunt needles, thereby avoiding repeated puncturing of surrounding tissue with sharp needles. While area cannulation is less frequently used, the BH and the rope ladder technique remain common clinical practices, each offering distinct advantages and limitations. Rope ladder cannulation is generally associated with lower infection and aneurysm rates; however, patients often report greater pain and an increased risk of hematoma formation [4, 9]. The repeated use of a preformed tunnel tract in BH cannulation reduces the incidence of hematomas and aneurysms, but has been linked to higher rates of both localized and systemic access-related bloodstream infections (ARBSIs) [10, 11]. These infections constitute the second leading cause of mortality among hemodialysis patients, who are inherently immunocompromised yet dependent on reliable vascular access [9, 12, 13]. A contributing factor to this elevated infection risk associated with BH cannulation is the placement of a polycarbonate (PC) thumbtack-shaped prototype, the BioHole™, within the tunnel tract during the first HD sessions [14]. These plug-like devices, featuring a circular head and tapered tail, as shown in Fig. 1B, are essential for

creating the tunnel tract within the first 7–14 days of BH cannulation [14]. Although the device can be removed once a stable tunnel has formed, its abiotic PC surface remains susceptible to bacterial colonization and subsequent biofilm formation [15].

Among the pathogens responsible for BH tract infections, *Staphylococcus aureus* accounts for more than 50% of reported cases, with approximately 42% of these infections caused by methicillin-resistant *S. aureus* (MRSA) [16, 17]. Other pathogens associated with BH tract infections include *Enterococcus faecalis*, *Escherichia coli*, and *Pseudomonas aeruginosa*, the latter being more prevalent in burn wound patients [16]. A common misconception is that BH-related infections arise primarily from improper needling technique. In practice, *S. aureus* is often transferred from the nasal cavity to the skin surrounding the vascular access site via the patient's hands, facilitating entry into the bloodstream and potentially leading to ARBSIs [17–19]. To mitigate this risk, nephrology units have implemented several preventive hygiene measures, including skin disinfection, sterile scab removal, and cannulation performed by trained personnel [20, 21]. Although these practices have significantly reduced the incidence of BH tract infections, their persistent occurrence highlights the need for the development of more effective infection-prevention strategies regarding BH cannulation using the BioHole™ device.

This study reports the development of an antibacterial coating for BioHole™ BH devices. BH devices composed of PC were first functionalized with amino groups through an environmentally friendly aqueous amination process, followed by the deposition of a layer-by-layer (LbL) coating designed to confer antibacterial properties. The antibacterial component in this polyelectrolyte system consisted of in-house generated silver nanoparticles (AgNPs) capped with negatively charged tannic acid (TA) and/or citrate (CI). Application of this antibacterial layer to the abiotic surface reduced the bacterial adhesion, thereby lowering the risk of BH tract-related infections. Additionally, various chemical reduction pathways for AgNPs synthesis were investigated, yielding uniform, nanosized, and monodisperse nanoparticles with antibacterial activity in the micromolar range. Overall, this study establishes a link between material engineering and a clinically relevant challenge in nephrology, and introduces a promising surface modification strategy to reduce the risk of BH tract-related infections.

2. Results

2.1. Silver nanoparticle characterization

2.1.1. Spectroscopic analysis of silver nanoparticles

UV–Vis spectrophotometric analysis confirmed the presence of AgNPs in both the in-house synthesized and commercial AgNPs, as evidenced in Fig. 2 by distinct SPR peaks within the 400–500 nm range [22]. The SPR peaks, corresponding to electron oscillations at the nanoparticle surface, were located at 428 ± 12 nm for CI-capped AgNPs, 398 ± 5 nm for CI/TA-capped AgNPs and 403 ± 2 nm for commercial AgNPs (n = 6). The CI-capped AgNPs exhibited pronounced tailing and a red-shifted SPR peak, likely resulting from the higher $AgNO_3$ concentration used during synthesis, which promotes the formation of larger

particles and increased aggregation [22–26]. Additionally, the commercial AgNPs displayed a lower absorbance maximum (≈ 1.5) compared to the in-house synthesized samples (3–4), confirming a lower nanoparticle concentration in the commercial formulation [24].

Visually, the CI-capped samples underwent a clear color transition from faint yellow (0–4 min) to orange (4–8 min) and finally to an opaque brownish hue (12–30 min), consistent with progressive nanoparticle nucleation and growth. The CI/TA-capped samples followed a similar trend, showing a bright yellow color at 4 min that rapidly deepened to dark orange (8 min) and dark transparent brown (12–40 min). The commercial AgNPs suspension retained a stable light-yellow appearance. These visual transitions were consistent with the UV–Vis spectra, where the CI-capped system reached its maximum absorbance after 20 min and the CI/TA-capped system after 12 min. This timing reflects the point of maximal reductive activity of the system, corresponding to the complete reduction of Ag^{+} ions to metallic Ag^{0}.[24]

2.1.2. Silver nanoparticles show strong anti-*Pseudomonas* and moderate anti-*Staphylococcus* activity

The antibacterial activity of both in-house synthesized and commercial AgNPs was evaluated against *S. aureus* and *P. aeruginosa*, representing clinically relevant Gram-positive and Gram-negative pathogens, respectively. To determine the optimal reduction time for maximal antibacterial efficacy, AgNPs synthesis was halted at 4, 8, or 30 minutes, corresponding to early, mid, and complete reduction stages based on UV-Vis data. As summarized in Table 1, nanoparticles from all three time points exhibited antibacterial activity in the low micromolar range. For both CI-capped and CI/TA-capped AgNPs, shorter reduction times yielded particles with enhanced antibacterial activity against both bacterial strains. Moreover, the in-house synthesized AgNPs demonstrated greater efficacy against *P. aeruginosa* than *S. aureus*, a trend also observed for the commercially obtained AgNPs. However, commercial particles showed lower activity overall, with an average IC_{50} value of 22 μM, compared to 8.5 μM and 9 μM for the CI-capped and CI/TA-capped AgNPs produced with a 4-minute reduction time, respectively. Based on these findings, CI-capped and CI/TA-capped AgNPs synthesized with a short 4-minute reduction time were selected for further experiments.

Table 1

IC_{50} values (concentrations causing 50% growth inhibition), MIC (minimum inhibitory concentration), and MBC (minimum bactericidal concentration) values against S. aureus and P. aeruginosa obtained from two independent screenings, each consisting of three technical replicates. CI denotes citrate-capped AgNPs, while CI/TA refers to citrate/tannic acid-capped AgNPs. In both conditions, the reduction reaction was continued for either 4, 8 or 30 minutes. *The concentration of the commercial AgNPs suspension was 185 µM, therefore, the maximum testable concentration was 64 µM.

	Repeat	*S. aureus* (ATCC 6538)			*P. aeruginosa* (PA01)		
		MIC (µM)	IC50 (µM)	MBC (µM)	MIC (µM)	IC50 (µM)	MBC (µM)
CI 4 minutes	1	**32**	**25 ± 2**	**128**	**8**	**5 ± 3**	**32**
	2	**32**	**30 ± 3**	**128**	**16**	**12 ± 1**	**32**
CI 8 minutes	1	64	37 ± 6	128	16	15 ± 2	64
	2	32	20 ± 3	128	16	11 ± 1	32
CI 30 minutes	1	> 256	228 ± 5	> 256	128	92 ± 4	256
	2	256	119 ± 3	> 256	64	26 ± 7	128
CI/TA 4 minutes	1	**32**	**22 ± 2**	**128**	**16**	**6 ± 4**	**32**
	2	**32**	**45 ± 0**	**128**	**16**	**12 ± 0**	**32**
CI/TA 8 minutes	1	> 256	202 ± 17	> 256	128	99 ± 2	256
	2	256	132 ± 5	> 256	64	19 ± 6	256
CI/TA 30 minutes	1	> 256	260 ± 17	> 256	128	95 ± 3	> 256
	2	256	200 ± 22	> 256	128	45 ± 14	> 256
Commercial AgNPs	1	32	66 ± 10	> 64*	16	19 ± 6	> 64*
	2	32	47 ± 4	> 64*	16	25 ± 1	> 64*

2.1.3. Silver particles are nanosized and mostly uniformly distributed

The morphology and size distribution of the AgNPs were determined by transmission electron microscopy (TEM). Figure 3 shows images of in-house produced CI-capped and CI/TA-capped AgNPs, as well as commercial AgNPs. When analyzing AgNPs reduced and stabilized solely with CI, a higher degree of agglomeration was observed, with particles tending to form clusters rather than remaining as discrete nanoparticles. Within these clusters, single nanoparticles had an average diameter of 30.6 ± 17.8 nm (n = 50). Subsequently, CI/TA-capped AgNPs were more monodisperse with an average diameter of 27.8 ± 6.4 nm and less agglomeration occurred between the particles (n = 50). Lastly, the commercial CI-capped AgNPs exhibited well-dispersed, distinct single AgNPs with an average diameter

of 13.0 ± 4.0 nm, representing the smallest size among all samples (n = 50). This value aligns with the specifications provided by Sigma-Aldrich (≈ 10 nm).

2.2. Hexamethylenediamine uniformly aminates the polycarbonate surface

To enable the electrostatic deposition of anionic AgNPs onto an inert PC surface, the substrate was first activated with cationic moieties. Figure 4 depicts the urethane formation mechanism when PC is treated with HMDA and the effectiveness of this activation under different solvents and treatment durations was evaluated by CBB staining [27]. Although all staining conditions affected the PC surface, a 30 min treatment in ddH_2O proved to be the most effective. In contrast, a 30 min treatment using an IP/ddH_2O mixture produced a lighter blue stain, indicating fewer available cationic amino groups. Prolonged treatment durations of 24 hours resulted in a cracked surface morphology, likely due to uneven distribution of amino groups or potential damage to the PC substrate caused by the prolonged HMDA treatment.

Aminated PC BioHole™ devices were subsequently coated using a LbL assembly process (Fig. 5), with in-house synthesized CI- or CI/TA-capped AgNPs serving as anionic building blocks and PLL as the cationic counterpart. Commercial AgNPs were excluded from this step onwards because of their limited *in vitro* antibacterial activity. PLL was selected as the cationic layer owing to its dual benefit of intrinsic antibacterial activity and established biocompatibility, making it suitable for biomedical surface modification [28, 29].

2.3. Coated BioHole™ devices show strong anti-*Pseudomonas* and moderate anti-*Staphylococcus* activity

The antibacterial performance of the coated BioHole™ devices was evaluated using the same bacterial strains as in the antibacterial activity assays. As shown in Fig. 6, the adhesion of both *S. aureus* and *P. aeruginosa* on the PC surface within 3 h was assessed. *P. aeruginosa* shows an adhesion of 1.4×10^6 and 2.4×10^6 CFU/mL for uncoated BioHole™ devices and HMDA aminated devices respectively. The adhesion of PAO1 on both CI-coated and CI/TA-coated BioHole™ devices did not reach the quantification limit of 1.0×10^2 CFU/mL. Subsequently, the adhesion of *S. aureus* on the different BioHole™ devices was quantified, yielding values of 1.6×10^6, 1.3×10^6, 2.8×10^4, and 2.1×10^4 CFU/mL for the uncoated, HMDA-treated, CI-coated, and CI/TA-coated samples, respectively.

2.4. The produced antibacterial BioHole™ device is biocompatible

In addition to AgNPs characterization and antibacterial evaluation of the coated medical devices, biocompatibility assessment is essential for medical device development. According to the ISO

standards for medical devices (ISO 10993), three main biocompatibility tests are advised when developing new medical devices: cytotoxicity, sensitization and irritation[30, 31]. While the last two are relevant at the later development stages, cytotoxicity is a prerequisite for further biological evaluation [32]. Therefore, an extraction-based cytotoxicity part was conducted on L-929 fibroblasts, by incubating the coated devices for 24 h in physiological medium [31].

To determine the viability of fibroblasts after extract exposure, a resazurin-based fluorometric assay was conducted. As shown in Fig. 7, neither uncoated BioHole™ devices nor coated variants affected fibroblast viability compared to the negative control. The positive control containing 10% SDS achieved a cell viability of less than 0.4%, which is classified by the ISO 10993-5 as cytotoxic, since it is below the threshold of 70% [30, 33]. These results indicate that coated BioHole™ devices are highly biocompatible, demonstrating that the incorporated AgNPs provided antibacterial efficacy without any detectable cytotoxicity.

3. Discussion

Although infections associated with BH cannulation and the use of the BioHole™ medical device are clinically relevant, data on their frequency and underlying mechanisms remains limited. A meta-analysis by Muir et al. reported a threefold increase in AVF infection rates associated with BH cannulation and data from the National Healthcare Safety Network, published by Lyman et al., similarly indicated an elevated risk of ARBSIs linked to this technique [16, 34, 35]. Various preventive measures; including proper skin disinfection, careful scab removal, staff training and the use of antimicrobial ointments such as bacitracin/polymyxin gauze pads or mupirocin calcium ointments; have reduced infection rates [36, 37].

A promising yet unexplored approach is the development of an antibacterial coating for BioHole™ devices to prevent bacterial colonization in the BH tract. In this study, AgNPs were synthesized in-house using either CI-based or CI/TA-based reduction systems. Both UV–Vis analysis (Fig. 2) and TEM characterization (Fig. 3) confirmed successful formation of nanoparticles following chemical reduction. CI-capped AgNPs, were approximately 3 nm larger than CI/TA-capped AgNPs by TEM and showed a higher degree of agglomeration. This was consistent with the tailing of a red-shifted SPR peak in UV-Vis spectra and visual appearance, as the solution exhibited a more opaque hue rather than remaining clear. The larger particle size of CI-capped AgNPs can be attributed to the higher concentration of silver salt precursor used [38]. The CI/TA-capped system demonstrated smaller particle size and improved monodispersity [39, 40]. These observations with TA addition have been documented by Ranoszek-Soliwoda et al., who reported that, in the presence of CI, TA is oxidized to quinone groups that form a stable complex with the nanoparticles [41]. Lastly, it is well established that smaller nanoparticles generally exhibit stronger antibacterial activity due to their higher surface-area-to-volume ratio [38, 42]. This trend, however, was not observed when comparing the in-house synthesized AgNPs (≈ 30 nm) with commercial AgNPs (≈ 10 nm), as shown in Table 1. One likely explanation for this discrepancy is the lower nanoparticle concentration in the commercial formulation. Both in-house formulations

demonstrated greater efficacy against *P. aeruginosa* than *S. aureus*, which could be attributed to the thick peptidoglycan layer and teichoic acid-rich cell wall, characteristic of Gram-positive cells [43, 44]. Gram-negative bacteria furthermore have negatively-charged lipopolysaccharides on their surface, which promote the adhesion of AgNPs [45]. One potential improvement to enhance antibacterial efficacy would have been to cap the AgNPs with cationic components, which has been shown to improve antibacterial effect, as demonstrated by Abbas et al [42]. However, this approach was not feasible in our study, because the LbL system required anionic capped particles.

In the next step, the PC BioHole™ device was aminated using an eco-friendly aqueous process adapted from VanDelinder et al [27]. This functionalization was a crucial prerequisite for initiating the deposition of a polyelectrolyte multilayer coating via dip-coating. Although the LbL approach is well-established, its application on BioHole™ devices combined with HMDA amination is innovative [46, 47]. The fundamental principles of this layered coating may be long established, yet they remain central to the emerging concept of architectonics, which holds significant promise as a leading strategy in nanomedicine [48]. Incorporation of in-house produced AgNPs into polyelectrolyte layers resulted in a coated BioHole™ device with significant antibacterial properties, as shown in Fig. 6. While a complete inhibition of bacterial adhesion was observed for *P. aeruginosa*, the activity against *S. aureus* was significant, yet limited to an approximate 2-log reduction. This outcome is consistent with the intrinsic antibacterial activity observed for the nanoparticles themselves. Furthermore, the coated medical devices exhibited no cytotoxicity toward L-929 fibroblasts, despite the well-documented cytotoxicity of free AgNPs [49]. This favorable outcome may be partly attributed to the use of an extract-based assay, in which the release of Ag^0 is likely reduced due to the absence of direct cell–material interactions [50]. Additionally, Bilal et al. reported the use of AgNPs within LbL constructs without inducing cytotoxicity toward L-929 fibroblasts, and similarly, Szaleniec et al. observed no cytotoxic effects when employing biocompatible TA as a nanoparticle stabilizer [51, 52].

4. Conclusion

This study successfully developed an antibacterial coating for BioHole™ BH devices to reduce infection incidence following BH cannulation and lower the risk of ARBSIs. Monodisperse and nanosized AgNPs with strong antibacterial activity were synthesized in-house using either CI-based or CI/TA-based chemical reduction systems. Following HDMA surface amination, the rigid PC BioHole™ devices were coated using a LbL dip-coating approach. The resulting coatings demonstrated a pronounced antibacterial efficacy against Gram-negative bacteria and a moderate yet significant effect against Gram-positive pathogens, while maintaining excellent biocompatibility towards L-929 fibroblasts. In conclusion, these findings highlight the potential of this AgNP-based coating as a preventive strategy to mitigate infection-related complications associated with BH cannulation in HD patients.

5. Materials & Methods

5.1. Materials

The bacterial strains *P. aeruginosa* ATCC 1596 (PA01) and *S. aureus* subsp. *aureus* Rosenbach ATCC 6538 were obtained from the ATCC (American Type Culture Collection, Manassas, VA, USA). CI, TA, acetic acid, silver nitrate ($AgNO_3$), hexamethylene diamine (HMDA), isopropanol (IP), methanol, sodium dodecyl sulfate (SDS), poly-L-lysine (PLL) and Luria Bertani (LB) agar and broth were purchased from Merck (Darmstadt, Germany). Commercial CI-capped AgNPs, Dulbecco's Phosphate-Buffered Saline (DPBS), pure ethanol, Dulbecco's Modified Eagle Medium (DMEM), L-glutamine, heat-inactivated fetal bovine serum (iFBS) and penicillin-streptomycin were obtained from Thermo Fisher Scientific (Waltham, MA, USA). The Coomassie Brilliant Blue R-250 (CBB) staining solution was prepared using reagents from Bio-Rad Laboratories (Hercules, CA, USA). Polystyrene well plates were purchased from Greiner Bio-One (Kremsmünster, Austria) and Mueller Hinton broth (MHB) was bought from Becton Dickinson (Franklin Lakes, NJ, USA). Lastly, BioHole™ BH devices (Nipro Co., Osaka, Japan) and their PC prototype mock-ups were supplied respectively via the Antwerp University Hospital (UZA) and the Antwerp Design Factory.

5.2. Silver nanoparticle production

AgNPs were synthesized via either a CI-based reduction or a dual-reductant system combining CI and TA. For the CI-based reduction, 4 mL of a 1% (m/v) CI solution was added dropwise to 50 mL of a boiling 1 mM $AgNO_3$ solution. The reaction was continued under magnetic stirring for varying durations (0–40 minutes) at 90°C and was terminated by placing the flask on ice. The CI/TA reduction involved a preconditioning step in which 6 mL of a 1% (m/v) CI solution and 1.2 mL of a 0.02 mM TA solution were incubated in a water bath at 60°C for 3 h. Subsequently, 7.2 mL of the preconditioned mixture was added to 94 mL of a boiling 0.55 mM $AgNO_3$ solution. Similarly to the CI-only reduction, the reaction was terminated at various time points (0–40 minutes) by placing the flask on ice. All solutions for nanoparticle production were made in double-distilled water (ddH2O).

5.3. Silver nanoparticle characterization

5.3.1. UV-Vis spectroscopy

Formation of AgNPs in both synthesis routes was verified by monitoring the visual color change from colorless to yellow or brown. Samples collected at defined time points (0–40 min) were analyzed in triplicate in 96-well plates alongside a commercial CI-capped AgNP control to enable direct comparison. UV–visible spectra were recorded using a Tecan Spark® Cyto spectrophotometer over a wavelength range of 300–800 nm to assess surface plasmon resonance (SPR) characteristics and spectral tailing.

5.3.2. Transmission scanning electron microscopy

800 µl of each AgNPs sample was centrifuged at 3000 rpm for 5 min, 500 µl of the supernatant was removed and the pellet was resuspended in the remaining 300 µl. Subsequently, 1 µL of this nanoparticle solution was applied to glow-discharged 300 mesh carbon coated copper grids (EM Resolutions, Staffordshire, United Kingdom). Excess solution was removed using blotting paper. The samples were dried at room temperature and then imaged with a Tecnai G2 Spirit Bio TWIN microscope at 120 kV,

without staining. Resulting images were processed using FIJI software (ImageJ Version 1.54g, Java 1.8.0_345).

5.3.3. Antimicrobial activity assay

The antibacterial activity of the in-house synthesized nanoparticles was assessed against *P. aeruginosa* and *S. aureus*. Concentration ranges for CI-capped and CI/TA-capped AgNPs were 0.5–512 µM, whereas commercial citrate-capped AgNPs (reference) were tested between 0.05–64 µM due to a lower stock concentration (185 µM). Bacterial suspensions were prepared in MHB at inoculum densities of approximately 10^4 CFU/mL for *S. aureus* and 10^5 CFU/mL for *P. aeruginosa*. For each nanoparticle formulation, samples obtained after 4, 8, and 30 min of reduction were evaluated. Following a 16 h incubation, the minimum inhibitory concentration (MIC) was determined visually, and the minimum bactericidal concentration (MBC) was established by subculturing aliquots from wells without visible growth onto LB agar. The half-maximal inhibitory concentration (IC_{50}) was subsequently determined using a resazurin-based viability assay. Briefly, 20 µL of a 0.01% resazurin solution was added to each well, followed by incubation for 15 min (*S. aureus*) or 45 min (*P. aeruginosa*). Fluorescence was recorded at an excitation wavelength of 550 nm and an emission wavelength of 590 nm using a Tecan Infinite® F-PLEX microplate reader.

5.4. BioHole™ device amination & layer-by-layer construction

Firstly, the BioHole™ devices or their PC prototypes were cleaned and sterilized by sequential sonication in 1% (m/v) SDS for 10 min, absolute ethanol for 15 min and ddH2O for 10 min. Subsequently, in order to create a cationic aminated surface, BioHole™ devices were submerged in a 10% (m/v) HMDA solution at pH 12, prepared in ddH2O or a 50:50 (v/v) mixture of ddH2O and IP, for 30 min or 24 h at 80°C in a warm water bath. The amination reaction involves nucleophilic substitution of the carbonyl groups of PC by diamines, leading to urethane formation and finally chain scission. Afterwards, BioHole™ devices were rinsed with acidified ddH2O (pH 6) to ensure a positive charge on the primary amines of HMDA. Amination was confirmed by staining the PC prototypes with 0.1% (m/v) CBB R-250 in a solution containing 40% (v/v) ethanol and 10% (v/v) acetic acid for 1 h. Samples were then briefly rinsed with a destaining solution composed of 40% (v/v) methanol and 10% (v/v) acetic acid in ddH2O, followed by sequential immersion in the destaining solution for 1 h and in a 1:1 mixture of destaining solution and ddH2O for 2 h.

To prepare antibacterial polyelectrolyte multilayers, aminated BioHole™ devices were alternately immersed in 1 mL cationic and anionic solutions for 15 min per step in 48-well plates. The cationic solution consisted of 0.5 mg/mL PLL, while the anionic solution contained the negatively capped AgNPs, reduced at a concentration of 1 mM and 0.55 mM $AgNO_3$ for CI- and CI/TA-capped particles respectively. After each deposition, devices were rinsed twice with ddH2O. Multilayers were assembled to a total of 9.5 bilayers, ending with an AgNPs layer, followed by 1h vacuum drying of the coated devices.

5.5. Antibacterial assay of coated BioHole™ devices

The anti-adhesion capacity of the BioHole™ devices was tested by placing them in a bacterial suspension of either *P. aeruginosa* (PAO1) or *S. aureus* (ATCC 6538) at $5x10^6$ CFU/mL. After 3 h, the bacterial suspension was removed, the devices were washed twice with DPBS and transferred in 1 mL of fresh LB broth containing 0.05% (v/v) Tween 80. This was followed by vortexing (20 s), 15 min sonication and another vortex cycle (20 s). Subsequently, the obtained solutions were diluted and plated onto LB agar for viable plate count analysis.

5.6. Biocompatibility of coated BioHole™ devices

Cytotoxicity of the coated BioHole™ devices was evaluated using L-929 fibroblast cells, as recommended by ISO (International Organization for Standardization) 10993-5 guidelines [31]. Cells were cultured in DMEM supplemented with 5% (v/v) iFBS, 2 mM L-glutamine, and 2% (v/v) penicillin–streptomycin. For the assay, 96-well plates were seeded with 100 µL of a 2×10^5 cells/mL suspension and incubated for 24 h at 37°C in 5% CO_2 until ~ 80% confluency.

An extraction-based cytotoxicity test was performed by incubating coated BioHole™ devices in 225 µL of complete culture medium for 24 h at 37°C. Subsequently, 100 µL of the extract was transferred to fibroblast-seeded wells and incubated for another 24 h. Cell morphology was assessed by live-cell imaging (Tecan Spark® Cyto; offset = 15 µm), while viability was quantified using a fluorescence-based resazurin assay. After medium removal, 100 µL of fresh medium and 25 µL of 0.01% (w/v) resazurin solution were added and incubated for 4 h at 37°C. Fluorescence was recorded at 550 nm excitation and 590 nm emission using a Tecan Infinite® F-PLEX plate reader. The positive control consisted of culture medium supplemented with 10% (v/v) SDS and unmodified complete medium served as the negative control.

5.7. Statistical methods

Statistical analyses on bacterial counts were conducted on data transformed to the log10 scale using the software GraphPad Prism v10.6.1. The Shapiro–Wilk test was used to verify data normality. Since all data followed a normal distribution, a one-way analysis of variance (ANOVA) with a Dunnett post-hoc correction was employed for assessing significant differences.

Declarations

Competing interests

The author(s) declare no competing interests.

Funding

M.W. is financed by the FWO under grant number 11I5523N. This work also received financial support from the FWO under grant number W000921N. The TEM microscope used in this publication, i.e. Tecnai Spirit G2 Biotwin (AUHA-08-004) was funded by a Medium-scale research infrastructure grant of the FWO.

Author Contribution

M.W.: Conceptualization, Methodology, Validation, Formal analysis, Investigation, Data curation, Writing – original draft, Visualization, funding acquisition. L.V.M.: Methodology, Validation, Formal analysis, Writing – Review & editing, Visualization. F.V.: Conceptualization, Investigation, Writing – Review & editing. Z.B.: Methodology, Validation, Formal analysis, Investigation, Data curation, Visualization, Writing – Review & editing. L.D.V.: Data curation, Writing – Review & editing, Supervision L.V.C.: Conceptualization, Resources, Writing – Review & editing, Project administration, Funding acquisition. P.C.: Conceptualization, Resources, Writing – Review & editing, Supervision, Project administration, Funding acquisition.

Acknowledgement

The authors would like to thank ACAM, the microscopy core facility of the University of Antwerp, and Karen Sterck for their guidance and performance of the transmission electron microscopy experiments.

Data Availability

The datasets used and/or analysed during the current study are available from the corresponding author on reasonable request.

References

1. National Kidney Foundation & Hemodialysis (2024). https://www.kidney.org/kidney-topics/hemodialysis
2. National Kidney Foundation. Hemodialysis Access | Fistula, Graft, & Catheter. (2025). https://www.kidney.org/kidney-topics/hemodialysis-access
3. Lok, C. E., Yuo, T. & Lee, T. Hemodialysis Vascular Access: Core Curriculum 2025. *Am. J. Kidney Dis.* **85**, 236–252 (2025).
4. Sousa, C. N. et al. How to choose the appropriate cannulation technique for vascular access in hemodialysis patients. *Ther. Apheresis Dial*. **27**, 394–401 (2023).
5. Xu, F. et al. Multiple Single Cannulaton Technique for Puncturing Arteriovenous Fistulas: Randomized Comparison With Rope Ladder Technique Cannulation. *Hemodial. Int.* https://doi.org/10.1111/HDI.70000 (2025).

6. Wong, B. et al. Buttonhole Versus Rope-Ladder Cannulation of Arteriovenous Fistulas for Hemodialysis: A Systematic Review. *Am. J. Kidney Dis.* **64**, 918–936 (2014).
7. Parisotto, M. T. et al. Cannulation technique influences arteriovenous fistula and graft survival. *Kidney Int.* **86**, 790–797 (2014).
8. Misra, M. History of the Buttonhole Technique. *Contrib. Nephrol.* **186**, 1–12 (2015).
9. MacRae, J. M. Should Buttonhole Cannulation of Arteriovenous Fistulas Be Used? CON. *Kidney360* 1, 322 (2020).
10. Baena, L. et al. Establishing the buttonhole technique as a puncture alternative for arteriovenous fistulas. Experience of a centre over 3 years. *Nefrología (English Edition)*. **37**, 199–205 (2017).
11. Yin, H., Zhou, C., Yu, H. & Ren, W. The Beneficial Effects of the Buttonhole Technique Used for the Cannulation of Arteriovenous Fistula Among Hemodialysis Patients: A Literature Review. *Am. J. Nurs. Sci.* **10**, 185–190 (2021).
12. Murdeshwar, H. N., Agarwal, A., Anjum, F. & Hemodialysis *StatPearls - NCBI Bookshelf* (2023). https://www.ncbi.nlm.nih.gov/books/NBK563296/
13. Hasanoglu, I. et al. Surveillance of hemodialysis related infections: a prospective multicenter study. *Sci Rep* **12**, (2022).
14. King, J. Buttonhole Tunnel Tract Creation with the BioHole® Buttonhole Device. *Contrib. Nephrol.* **186**, 21–32 (2015).
15. Christensen, L. D. et al. Bacteriology of the Buttonhole Cannulation Tract in Hemodialysis Patients: A Prospective Cohort Study. *Am. J. Kidney Dis.* **72**, 234–242 (2018).
16. Lyman, M. et al. Risk of Vascular Access Infection Associated With Buttonhole Cannulation of Fistulas: Data From the National Healthcare Safety Network. *Am. J. Kidney Dis.* **76**, 82 (2020).
17. Glerup, R., Svensson, M., Jensen, J. D. & Christensen, J. H. Staphylococcus aureus Bacteremia Risk in Hemodialysis Patients Using the Buttonhole Cannulation Technique: A Prospective Multicenter Study. *Kidney Med.* **1**, 263–270 (2019).
18. Toma, S., Shinzato, T. & Hayakawa, K. Access-Related Infections Involving the Buttonhole Technique. *Blood Purif.* **41**, 306–312 (2016).
19. Di Nicolò, P., Cornacchiari, M., Mereghetti, M. & Mudoni, A. Buttonhole Cannulation of the AV Fistula: A Critical Analysis of the Technique. *Semin Dial*. **30**, 32–38 (2017).
20. Labriola, L., Crott, R., Desmet, C., Romain, C. & Jadoul, M. Infectious complications associated with buttonhole cannulation of native arteriovenous fistulas: a 22-year follow-up. *Nephrol. Dial Transpl.* **39**, 1000–1007 (2024).
21. Labriola, L., Crott, R. & Desmet, C. Infectious Complications Following Conversion to Buttonhole Cannulation of Native Arteriovenous Fistulas: A Quality Improvement Report. *J. Vasc Surg.* **54**, 1221 (2011).
22. Ider, M., Abderrafı, K., Eddahbi, A., Ouaskit, S. & Kassiba, A. Silver Metallic Nanoparticles with Surface Plasmon Resonance: Synthesis and Characterizations. *J. Cluster Sci.* **28**, 1051–1069 (2017).

23. Aziz, S. B., Abdullah, O. G., Saber, D. R., Rasheed, M. A. & Ahmed, H. M. Investigation of Metallic Silver Nanoparticles through UV-Vis and Optical Micrograph Techniques. *Int. J. Electrochem. Sci.* **12**, 363–373 (2017).
24. Nageeb, M., 1∗, R., Abdelrady, E. & Ghabrial, T. M. Microwave assisted green synthesis of silver nanoparticles using Trigonella Hamosa L.plant extract for the photodegradation of some water pollutants. *Sci. Rep.* **15**, 1–18 (2025).
25. Długosz, O. et al. Cleaner synthesis of betaine-based natural deep eutectic solvents and the effect of their composition on silver nanoparticle suspensions. *Ind. Crops Prod.* **233**, 121354 (2025).
26. De Leersnyder, I., De Gelder, L., Van Driessche, I. & Vermeir, P. Revealing the Importance of Aging, Environment, Size and Stabilization Mechanisms on the Stability of Metal Nanoparticles: A Case Study for Silver Nanoparticles in a Minimally Defined and Complex Undefined Bacterial Growth Medium. *Nanomaterials* **9**, 1684 (2019).
27. VanDelinder, V. et al. Simple, Benign, Aqueous-Based Amination of Polycarbonate Surfaces. *ACS Appl. Mater. Interfaces*. **7**, 5643–5649 (2015).
28. Lebaudy, E., Guilbaud-Chéreau, C., Frisch, B., Vrana, N. E. & Lavalle, P. The High Potential of ε-Poly-l-Lysine for the Development of Antimicrobial Biomaterials. *Adv. NanoBiomed Res.* **3**, 2300080 (2023).
29. Shu, D. et al. Biosynthetic ε-poly-L-lysine for the treatment of extensively- and pan-drug-resistant Pseudomonas aeruginosa. *npj Antimicrob. Resist.* **3**, 77 (2025).
30. Kanďárová, H. & Pôbiš, P. The Big Three in biocompatibility testing of medical devices: implementation of alternatives to animal experimentation—are we there yet? *Front. Toxicol.* **5**, 1337468 (2023).
31. International Organization for Standardization. Biological evaluation of medical devices — Part 5: Tests for in vitro cytotoxicity ((ISO Standard No. 10993-5:2009). (2009). https://www.iso.org/standard/36406.html
32. LI, W., XU, Y. & ZHOU, J. & Study of the in vitro cytotoxicity testing of medical devices. *Biomed. Rep.* **3**, 617–620 (2015).
33. Gruber, S. & Nickel, A. Toxic or not toxic? The specifications of the standard ISO 10993-5 are not explicit enough to yield comparable results in the cytotoxicity assessment of an identical medical device. *Front. Med. Technol.* **5**, 1195529 (2023).
34. Allon, M. Is It Time to Abandon Buttonhole Cannulation of Arteriovenous Fistulas? *Kidney Med.* **1**, 235–237 (2019).
35. Muir, C. A. et al. Buttonhole cannulation and clinical outcomes in a home hemodialysis cohort and systematic review. *Clin. J. Am. Soc. Nephrol.* **9**, 110–119 (2014).
36. Ball, L. K. The buttonhole technique: strategies to reduce infections. *Nephrol Nurs. J* **7**, (2010).
37. Vachharajani, T. J., Wong, L., Niyyar, V. D., Abreo, K. D. & Mokrzycki, M. H. Buttonhole Cannulation of Arteriovenous Fistulas in the United States. *Kidney360* 1, 306 (2020).

38. Duman, H. et al. Silver Nanoparticles: A Comprehensive Review of Synthesis Methods and Chemical and Physical Properties. *Nanomaterials* **14**, 1527 (2024).
39. Gangwar, C. et al. Silver nanoparticles fabricated by tannic acid for their antimicrobial and anticancerous activity. *Inorg. Chem. Commun.* **141**, 109532 (2022).
40. Huang, X. et al. One-step room-temperature synthesis of Au@Pd core–shell nanoparticles with tunable structure using plant tannin as reductant and stabilizer. *Green. Chem.* **13**, 950–957 (2011).
41. Ranoszek-Soliwoda, K. et al. The role of tannic acid and sodium citrate in the synthesis of silver nanoparticles. *J. Nanopart. Res.* **19**, 1–15 (2017).
42. Abbaszadegan, A. et al. The Effect of Charge at the Surface of Silver Nanoparticles on Antimicrobial Activity against Gram-Positive and Gram-Negative Bacteria: A Preliminary Study. *J. Nanomater.* 720654 (2015). (2015).
43. More, P. R. et al. Silver Nanoparticles: Bactericidal and Mechanistic Approach against Drug Resistant Pathogens. *Microorganisms* **11**, 369 (2023).
44. Anees Ahmad, S. et al. Bactericidal activity of silver nanoparticles: A mechanistic review. *Mater. Sci. Energy Technol.* **3**, 756–769 (2020).
45. Frippiat, T., Art, T. & Delguste, C. Silver Nanoparticles as Antimicrobial Agents in Veterinary Medicine: Current Applications and Future Perspectives. *Nanomaterials* **15**, 202 (2025).
46. Dube, E. & Okuthe, G. E. Silver Nanoparticle-Based Antimicrobial Coatings: Sustainable Strategies for Microbial Contamination Control. *Microbiol. Res.* **16**, 110 (2025).
47. Naveas, N. et al. Antibacterial Films of Silver Nanoparticles Embedded into Carboxymethylcellulose/Chitosan Multilayers on Nanoporous Silicon: A Layer-by-Layer Assembly Approach Comparing Dip and Spin Coating. *Int. J. Mol. Sci.* **24**, 10595 (2023).
48. Ariga, K. Layer-by-Layer Nanoarchitectonics: A Method for Everything in Layered Structures. *Mater. 2025*. **18**, 654 (2025).
49. Park, M. V. D. Z. et al. The effect of particle size on the cytotoxicity, inflammation, developmental toxicity and genotoxicity of silver nanoparticles. *Biomaterials* **32**, 9810–9817 (2011).
50. Sussman, E. M., Casey, B. J., Dutta, D. & Dair, B. J. Different cytotoxicity responses to antimicrobial nanosilver coatings when comparing extract-based and direct-contact assays. *J. Appl. Toxicol.* **35**, 631–639 (2015).
51. Bilal, M. et al. Development of silver nanoparticles loaded chitosan-alginate constructs with biomedical potentialities. *Int. J. Biol. Macromol.* **105**, 393–400 (2017).
52. Szaleniec, J. et al. Biocidal Activity of Tannic Acid-Prepared Silver Nanoparticles towards Pathogens Isolated from Patients with Exacerbations of Chronic Rhinosinusitis. *Int. J. Mol. Sci.* **23**, 15411 (2022).

Figures

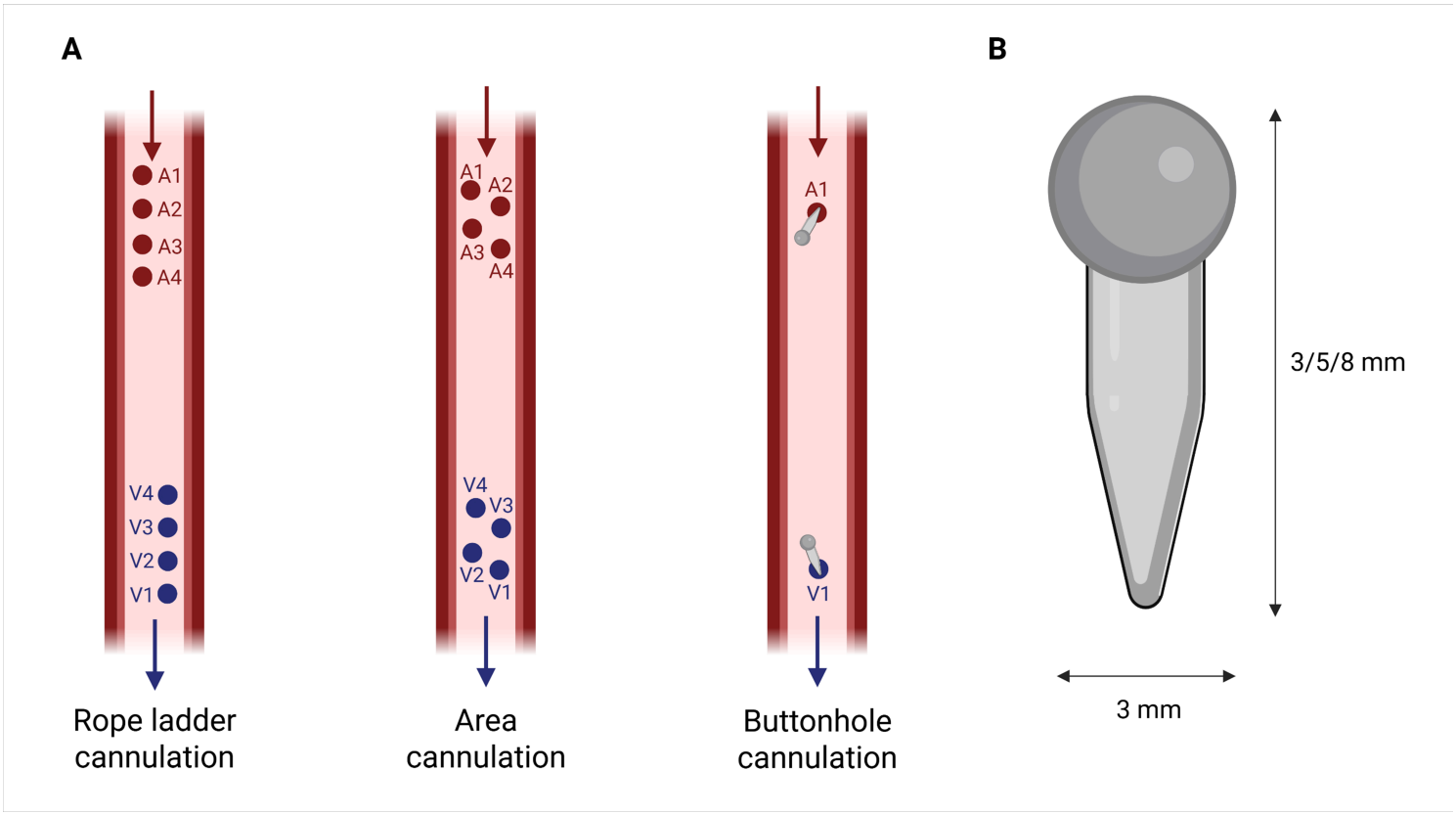

Figure 1

(A) *Different arteriovenous fistula cannulation techniques where 'A' represent the arterial puncture site and 'V' the venous puncture site* ***(B)*** *Polycarbonate BioHole™ buttonhole cannulation device [13].*

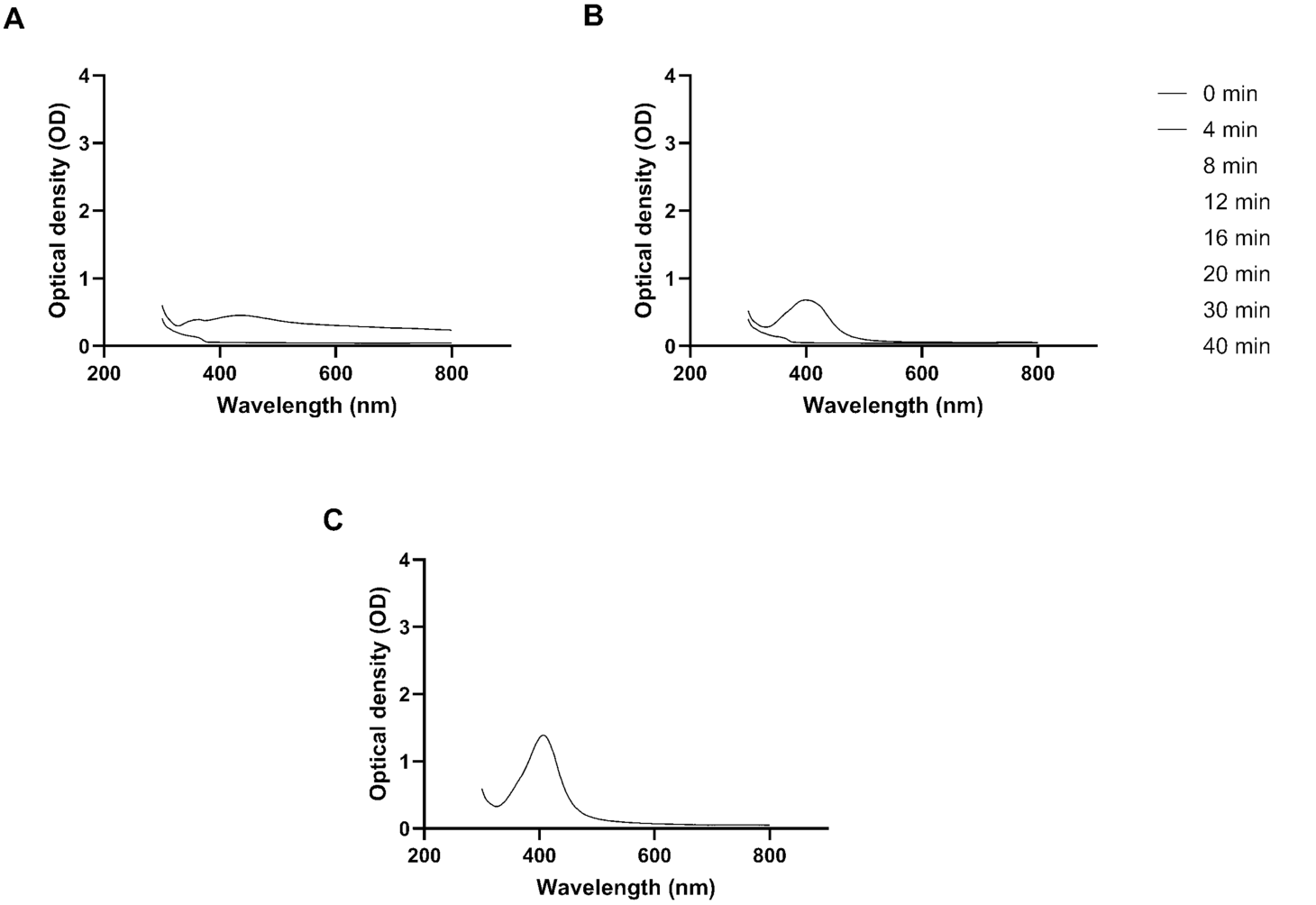

Figure 2

*UV-Vis spectra recorded at different reduction end points of **(A)** CI-capped AgNPs and **(B)** CI/TA-capped AgNPs. Panel **(C)** shows commercial CI-capped AgNPs. Samples were measured in biological duplicates and technical replicates.*

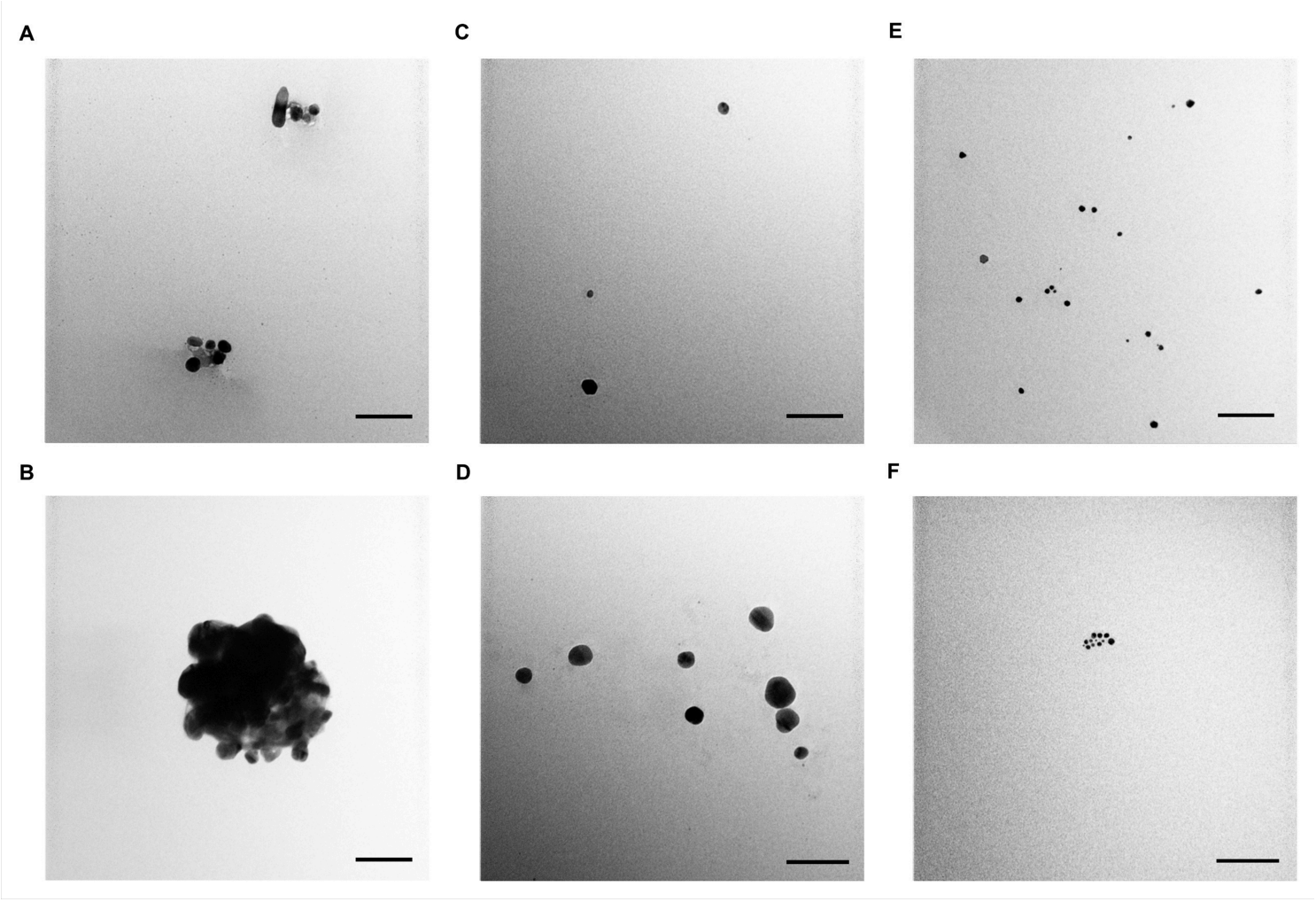

Figure 3

*Transmission electron microscopy images of **(A-B)** CI-capped AgNPs **(C-D)** CI/TA-capped AgNPs **(E-F)** commercial AgNPs. The reduction reaction was halted after 4 minutes for both CI-caped as CI/TA-capped AgNPs. All images are accompanied by a 100 nm scale bar.*

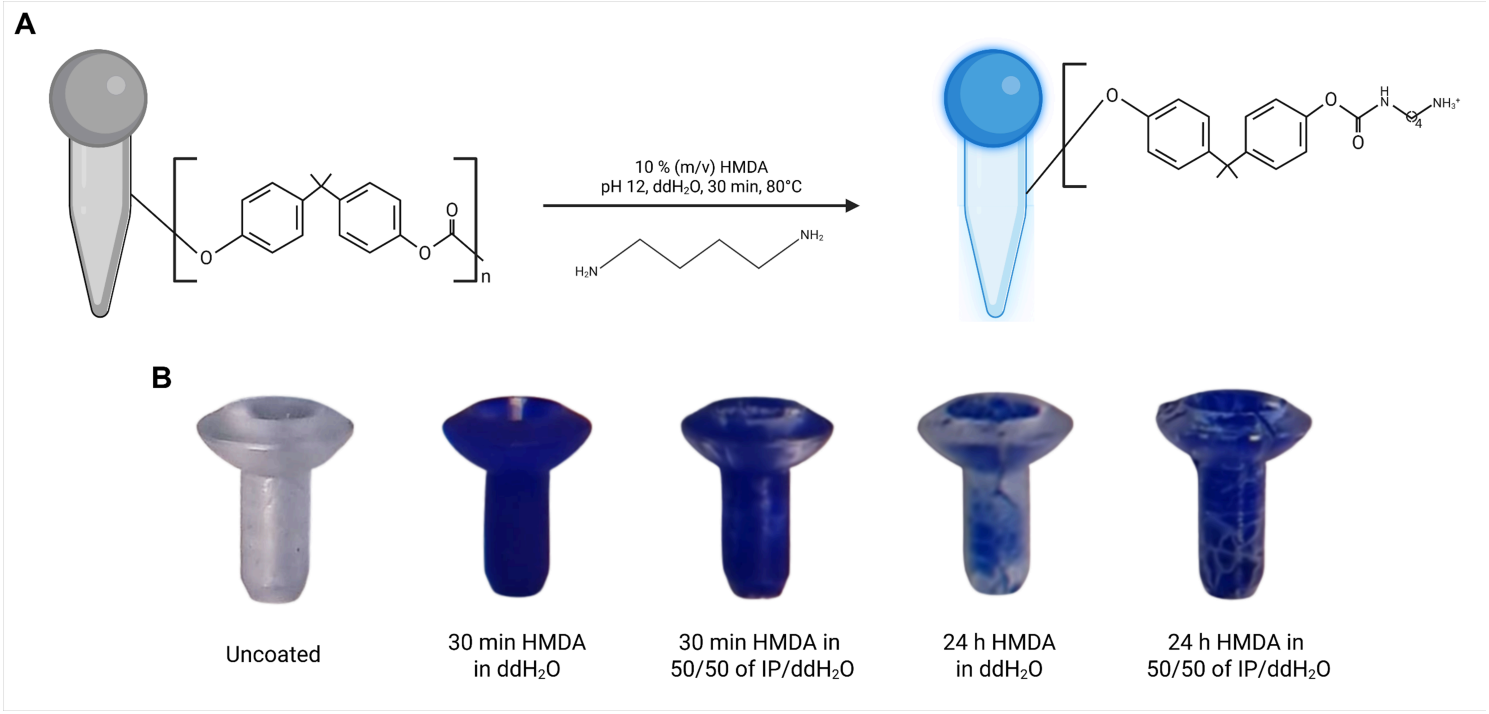

Figure 4

(A) *Amination mechanism of polycarbonate and* ***(B)*** *staining of free amino groups on polycarbonate prototypes with Coomassie Brilliant Blue.*

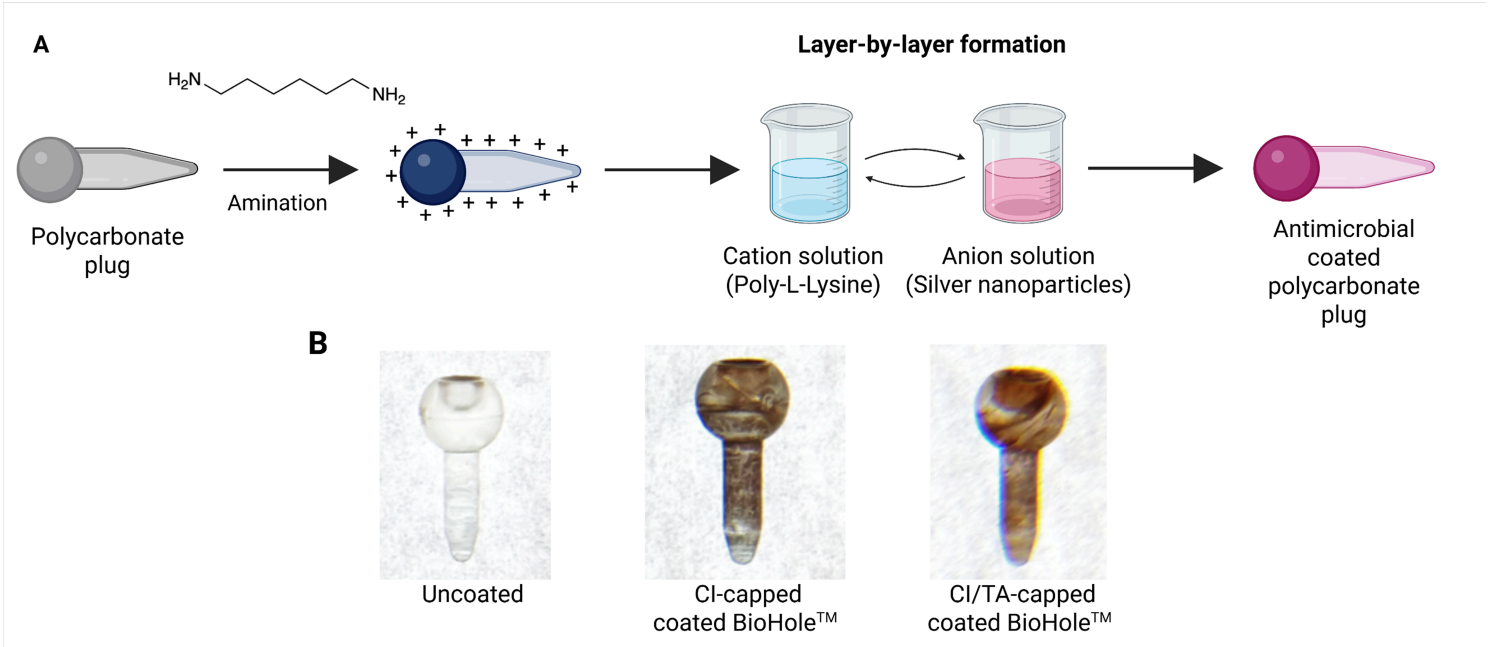

Figure 5

(A) *Amination and Layer-by-layer coating of BioHole™ devices* ***(B)*** *visual representation of coated BioHole™ devices.*

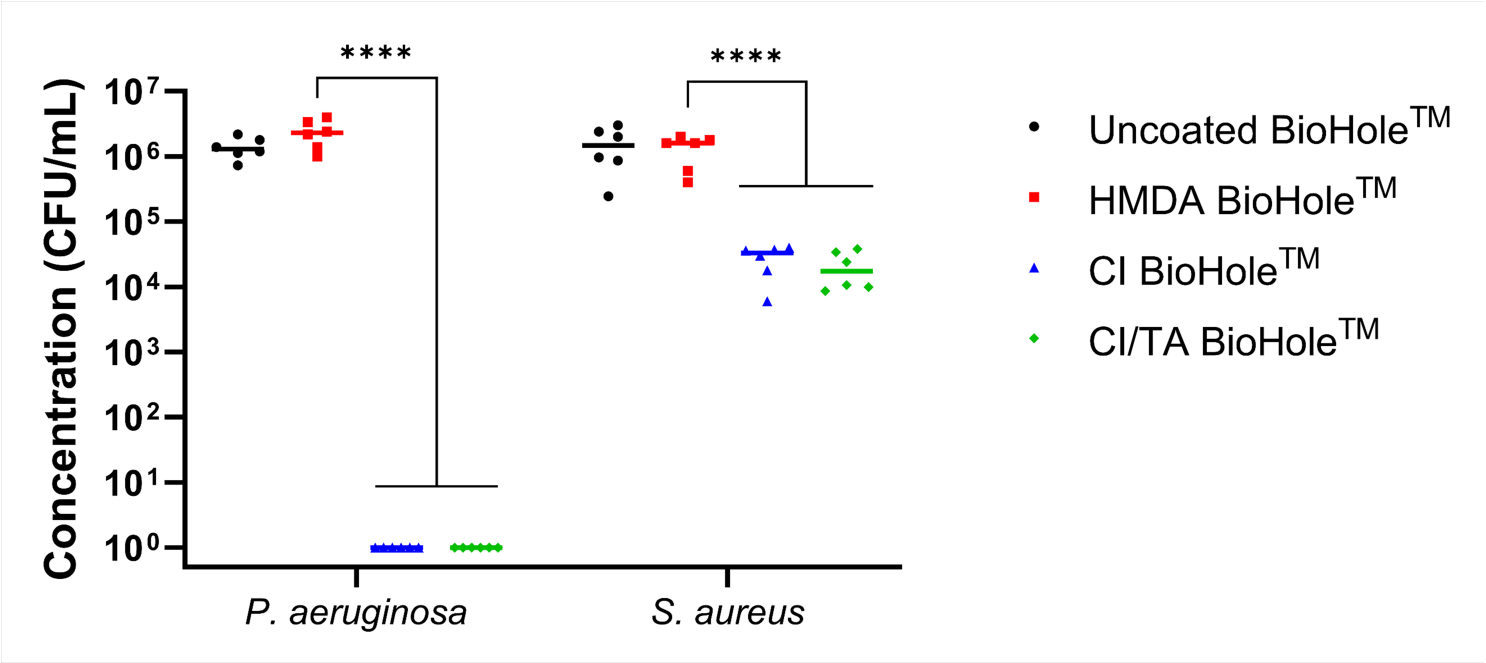

Figure 6

*Antibacterial evaluation of uncoated BioHole™ devices, hexamethylenediamine (HMDA) aminated BioHole™ devices and layer-by-layer coated BioHole™ devices with citrate-capped (CI) and citrate/tannic acid-capped (CI/TA) silver nanoparticles. Both experiments were performed in biological duplicate with three technical measurements each (n = 6). The mean and individual data points are shown. one-way analysis of variance (ANOVA) with a Dunnett post-hoc correction was employed for assessing significant differences (**** $p < 0.0001$).*

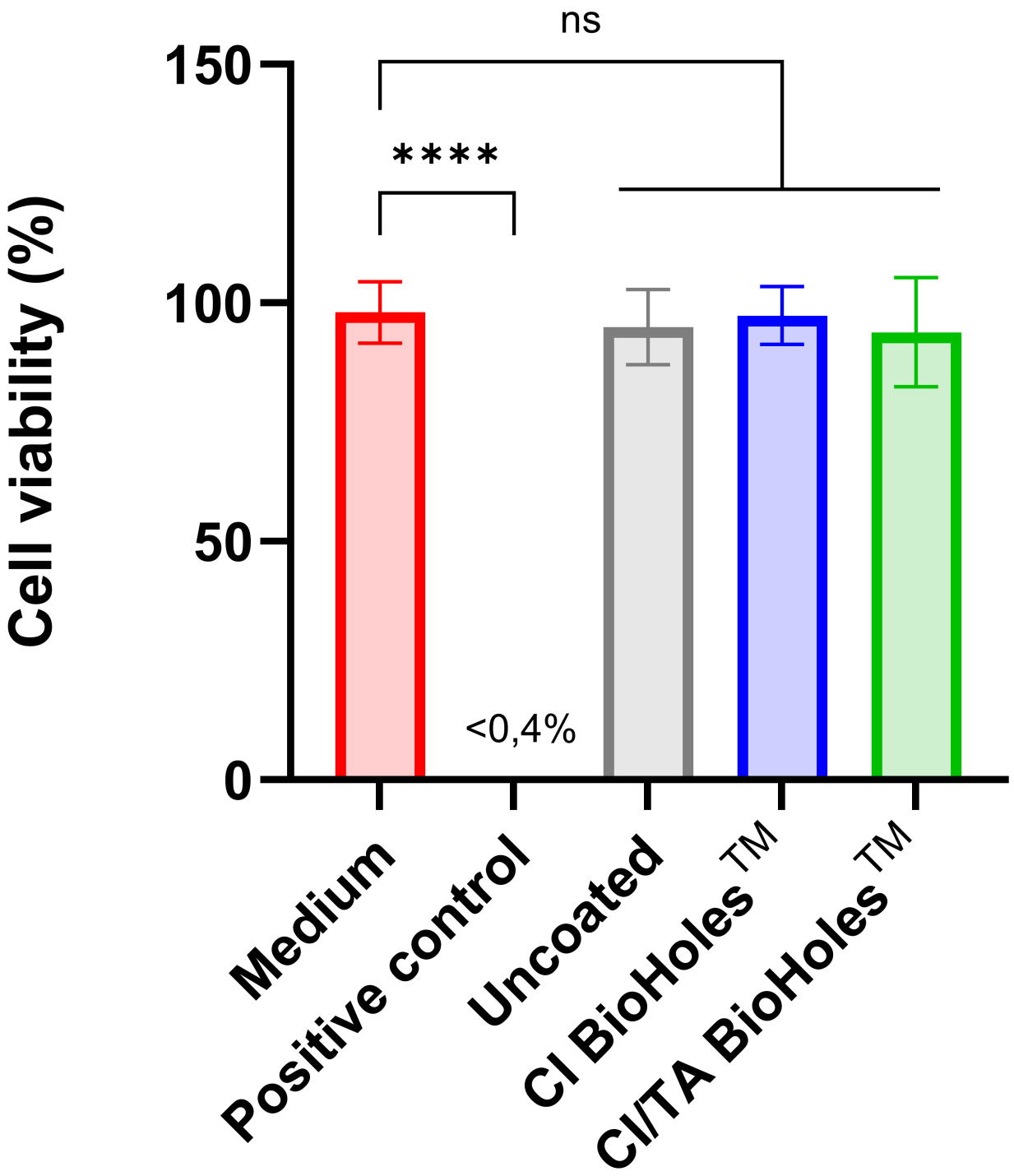

Figure 7

cytotoxicity evaluation of uncoated BioHole™ devices and layer-by-layer coated BioHole™ devices with citrate-capped (CI) and citrate/tannic acid-capped (CI/TA) silver nanoparticles. Viability of L-929 fibroblasts was assessed against extracts of the devices as recommended in ISO 10993-5 guidelines via a test on extracts. Normal medium was used as negative control and 10% sodium dodecyl sulphate (SDS) as a positive control. one-way analysis of variance (ANOVA) with a Dunnett post-hoc correction was employed

*for assessing significant differences (ns, not significant, $p > 0.05$ and **** $p \leq 0.0001$) and a cell viability below 70% was considered cytotoxic.*